Cell Death & Differentiation (2020) 27:3162–3176
https://doi.org/10.1038/s41418-020-0570-8

Cell Death & Differentiation

ARTICLE

RBMX is required for activation of ATR on repetitive DNAs to maintain genome stability

Tian Zheng[1] · Haoxian Zhou[1] · Xiaocui Li[1] · Di Peng[2] · Yiding Yang[1] · Yanru Zeng[2] · Haiying Liu[1] · Jian Ren[2] · Yong Zhao[1,2]

Received: 30 October 2019 / Revised: 15 May 2020 / Accepted: 20 May 2020 / Published online: 3 June 2020

Abstract

ATR is a master regulator of cell response to replication stress. Adequate activation of ATR is essential for preventing genome aberrance induced by replication defect. However, the mechanism underlying ATR activation is not fully understood. Here, we identify that RBMX is an ssDNA binding protein that orchestrates a novel pathway to activate ATR. Using super-resolution STORM, we observe that RBMX and RPA bind to adjacent but nonoverlapping sites on ssDNA in response to replication stress. RBMX then binds to and facilitates positioning of TopBP1, which activates nearby ATR associated with RPA. In addition, ATR activation by ssDNA-RBMX-TopBP1 is independent of ssDNA–dsDNA junction and 9-1-1 complex. ChIP-seq analysis reveals that RBMX/RPA are highly enriched on repetitive DNAs, which are considered as fragile sites with high replication stress. RBMX depletion leads to defective localization of TopBP1 to replication stressed sites and inadequate activation of ATR. Furthermore, cells with deficient RBMX demonstrate replication defect, leading to formation of micronuclei and a high rate of sister-chromatin exchange, indicative of genome instability. Together, the results identify a new ssDNA-RBMX-TopBP1 pathway that is specifically required for activation of ATR on repetitive DNAs. Therefore, RBMX is a key factor to ensure genome stability during replication.

Introduction

The maintenance of genomic integrity relies on accurate and complete DNA duplication. Eukaryotic genome is constantly challenged by assaults that may impede replication of DNA. The common nominator of replication stress is a stalled replication fork that triggers a genome surveillance pathway orchestrated by ATR (ataxia telangiectasia-mutated and Rad3-related) [1–5]. ATR is recruited to chromatin by RPA that coat the single-stranded DNA (ssDNA) in stalled replication forks. ATR and its downstream effectors then act to stabilize stalled forks and delay cell cycle progression [6, 7]. Therefore, ATR pathway is clearly essential to ensure proper and complete duplication of the genome during each cell division. Impaired ATR signaling leads to genome instability, developmental defects as well as accelerated aging [8–10].

One of the first steps in the cellular response to replication stress is activation of ATR. Both ssDNA and ssDNA–dsDNA junctions are present when DNA replication forks are challenged. RPA-coated ssDNA recruits ATR to chromatin through its obligatory binding partner ATR-interacting protein (ATRIP) [11]. ATR is then autophosphorylated or allosterically-activated by DNA topoisomerase 2-binding protein 1 (TopBP1) [12, 13]. TopBP1, which is primarily recruited by the 9-1-1 complex (Rad9-Hus1-Rad1) to ssDNA–dsDNA junctions, is proposed to play a major role in ATR activation [14]. Recent work identified Ewing's tumor-associated antigen 1 (ETAA1) as an activator of ATR in TopBP1 independent manner [15, 16]. However, ETAA1 primarily regulates

Edited by M. Oren

Supplementary information The online version of this article (https://doi.org/10.1038/s41418-020-0570-8) contains supplementary material, which is available to authorized users.

✉ Yong Zhao
zhaoy82@mail.sysu.edu.cn

[1] MOE Key Laboratory of Gene Function and Regulation, School of Life Sciences, Sun Yat-sen University, Guangzhou 510006, China

[2] State Key Laboratory of Oncology in South China, Collaborative Innovation Center for Cancer Medicine, Sun Yat-sen University Cancer Center, Guangzhou 510006, China

mitotic ATR signaling [17]. Despite of its importance, ATR activation is a complex process that is not fully understood. For example, the mechanism(s) that activates ATR at ssDNA–dsDNA junctions and in ssDNA region must be distinct; ATR activation on chromosomal fragile sites might be different from other locations; how ATR is activated in these sites remains to be elucidated.

RBMX, also known as hnRNP G, is originally recognized as a part of spliceosome and functions in alternative splicing [18–22]. Until recent years, RBMX is rediscovered to participate in DNA damage repair, cohesion of sister chromatids, and the assembling of higher-order ribonucleoprotein complex for promoting genomic stability [23–25]. Despite these links, it remains elusive if RBMX is involved in ATR-mediated DNA damage response (DDR). Here, we provide evidence that RBMX plays a novel role in activating ATR in response to replication stress. RBMX often localizes to repetitive DNAs of genome upon replication stress, where RBMX binds to ssDNA adjacent to RPA via its RBM1CTR domain. Meanwhile, RBMX interacts with TopBP1. Therefore, RBMX activates ATR recruited by RPA in TopBP1-dependent, but 9-1-1 complex-independent manner. These results uncover a new mechanism for activation of ATR and support the idea that RBMX plays an indispensable role in promoting genome stability in human cells.

Materials and methods

Cell culture and transfection

293T, HeLa, and U2OS cells were obtained from American Type Culture Collection (Manassas, VA). All cells were grown in DMEM (GIBCO) with 10% fetal bovine serum (GIBCO) and 100 U/ml penicillin/streptomycin (GIBCO). Cells were cultured at 37 °C and 5% CO_2. All the cells were verified by standardized short tandem repeat analysis. Mycoplasma was regularly examined during cell culturing, and no contamination occurred during this study. Plasmid DNA was transiently transfected into 293T cells using the PEI method: plasmid DNA was incubated with PEI for 15 min, added to cells at appropriate confluence (50–60%) and incubated for 6 h. The medium was exchanged for fresh medium, and cells were incubated for 48 h. siRNAs transfections were performed with RNAiMAX (Thermo Fisher Scientific). siRNA sequences: RBMX-1:5′-UGCUUCAAGAGCUUUCUCA-3′; RBMX-2:5′-UUCAUCAAGAGUACUUCCA-3′; Rad9A:5′-GAAGAACAGUGAGCGGAAC-3′; Rad17:5′-GACAAAGUAUAACAAGUUA-3′; TopBP1: 5′-AGACCUUAAUGUAUCAGUA-3′; ATR: 5′-GCCGCUAAUCUUCUAACAU-3′; RPA: 5′-GCCUGGUAGCCUUUAAGAU-3′

Reagents and plasmids

Camptothecin (CPT) was purchased from MCE (Shanghai, China). RNase A and DNase I were purchased from Takara (Beijing, China). Rec J_f and ExoI were purchased from NEB (USA). Wild-type RBMX, TopBP1, ATRIP, RPA1, and Rad9A genes were amplified from 293T mRNA and cloned into pLenti-HA/Flag. The siRNA-resistant RBMX was generated by synonymously mutating the sequences at siRNA targeting site based on wild-type RBMX.

Immunofluorescence

For immunofluorescence experiments, cells plated on coverslips were fixed in cold methanol and permeabilized with 0.2% Triton. The coverslips were incubated sequentially with primary antibody and fluorescence-labeled secondary antibody. Coverslips mounted with Vectashield mounting medium containing DAPI (Vector Laboratories) were visualized and analyzed using fluorescence microscopy. Antibodies used: 53BP1 (1:2000, NB100-304, Novus Biologicals), RPA1 (1:100, sc-28304, Santa Cruz), RBMX (1:250, ab190352, abcam), TopBP1 (1:100, sc-271043, Santa Cruz), TopBP1 (1:500, ab2402, abcam), PCNA (1:400, ab92552, abcam).

Stochastic Optical Reconstruction Microscopy (STORM)

Super-resolution images were acquired with STORM system established by NBI (NanoBioImaging Ltd.) specifically designed for dual-channel imaging of AlexaFluor647- and AlexaFluor750-immunolabeled samples, as previously reported [26]. Cells were grown on a coverslip immobilized with polystyrene particles (Spherotech), fixed in cold methanol for 10 min on ice, followed by incubation at the room temperature for 10 min in 0.2% Triton X-100. The coverslip was washed and incubated with blocking solution for 1 h at the room temperature, washed with PBS, and then incubated with blocking solution containing dye-conjugated primary antibody for 1 h at the room temperature. The coverslip was washed, incubated in 4% paraformaldehyde for 10 min, and then washed with PBS. Each super-resolution image was reconstructed by Fiji from a movie containing 10,000 frames, during which time the dye molecules briefly cycled from dark to bright and back again for many iterations in TCEP-containing imaging buffer.

Immunoblotting

Proteins were separated with SDS-PAGE and transferred to PVDF membrane. The following antibodies were incubated

with membrane: ATR (1:5000, ab2905, abcam), ATR pT1989 (1:1000, GTX128145, GeneTex), RBMX (1:1000, ab190352, abcam), RPA34 (1:400, MABE285, Millipore), CHK1 pS345 (1:1000, 2348T, Cell Signaling Technology), CHK1 (1:200, sc-56291, Santa Cruz), Flag (1:2000, F1804, Sigma Aldrich), GFP (1:2500, ab290, abcam), TopBP1 (1:100, sc-271043, Santa Cruz), Rad17 (1:100, sc-17761, Santa Cruz), α-tubulin (1:2000, 66031-1-Ig, Proteintech), GAPDH (1:5000, 60004-1-Ig, Proteintech), HRP-conjugated anti-rabbit or anti-mouse secondary antibodies (KPL, Inc) were then used.

RNA extraction and real-time quantitative RT-PCR

Total RNA was extracted using RNAiso Plus (Takara) according to the manufacturer's instructions. cDNA was synthesized with PrimeScript II first-strand cDNA Synthesis Kit (Takara), followed by amplification with RealStar Power SYBR Mixture (GenStar). qPCR was performed with a LightCycler 480 Real-Time PCR system (Roche). Data were analyzed using the comparative Ct ($2-\Delta\Delta Ct$) method [27]. All experiments were performed in triplicate. qPCR primers for mRNA detection were as follows: β-actin-forward 5′-CATGTACGTTCCTATCCAGGC-3′; β-actin-reverse 5′-CTCCTTAATGTCACGCACGAT-3′; TopBP1-forward 5′-TTCAGCAACTCACAGTTAAGCA-3′; TopBP1-reverse 5′-GGCACACTCATACTTCTGACC-3′; RPA1-forward 5′-GTGGACCATTTGTGCTCGTG-3′; RPA1-reverse 5′-TTCGTCAACCAGTTCTAGGGA-3′; ATR-forward 5′-TCCCTTGAATACAGTGGCCTA-3′; ATR-reverse 5′-TCCTTGAAAGTACGGCAGTTC-3′; CHK1-forward 5′-ATATGAAGCGTGCCGTAGACT-3′; CHK1-reverse 5′-TGCCTATGTCTGGCT CTATTCTG-3′; RBMX-forward 5′-TGGAAGCAGTCGCTATGATG-3′; RBMX-reverse 5′-GAGGGTACCCCCTTTCCATA-3′.

Viability assays

Viability assays were performed in HeLa cells transfected with indicated siRNA(s). Cells were treated with increasing concentrations of drug and viability was measured 24 h later with CCK-8 (Biotool). All viability measurements are presented as a percentage of the untreated siNC cells.

Co-immunoprecipitation

293T cells were transfected with plasmids and cell lysates were prepared using RIPA buffer (1% NP-40, 0.25% Sodium Deoxycholate, 50 mM Tris-HCl (pH 7.4), 150 mM NaCl, 1 mM EDTA). Flag-tagged proteins was immunoprecipitated using Flag antibody conjugated to protein G Dynabeads (Sigma). Coprecipitating proteins were identified by SDS-PAGE followed by immunoblotting. Endogenous immunoprecipitation was performed by incubating 293T or HeLa cell extracts with primary antibody overnight. Protein A/G agarose beads (Santa Cruz) were then used to capture the antigen–antibody complex. Following primary antibodies were used: TopBP1 (ab2402, abcam), Rad17 (sc-17761, Santa Cruz).

Sister chromatid exchange assays

Cells transfected with siRNAs were labeled with 10 μM BrdU for two cell cycles. Colcemid was added to a final concentration of 150 ng/ml for 1 h and cells were harvested. Cells were stained with 0.1 mg/ml acridine orange, mounted in Sorenson buffer (pH6.8, 0.1 M Na_2HPO_4, 0.1 M NaH_2PO_4), visualized by fluorescence microscopy.

Comet assay

Cells transfected with siRNA were harvested and mixed with 0.5% low melting temperature agarose and layered on slides pre-coated by 1.5% normal agarose. Slides were lysed in 2.5 M NaCl, 100 mM EDTA, 10 mM Tris (pH 8.0), 0.5% Triton X-100, 3% DMSO, 1% N-lauroylsarcosine overnight at 4 °C and then electrophoresis in 300 mM sodium acetate, 100 mM Tris-HCl, 1% DMSO at 1.5 V/cm for 20 min. After neutralization with 0.4 M Tris-HCl (pH 7.3), slides were washed and dried with ethanol. The slides were then mounted with Vectashield mounting medium containing DAPI (Vector Laboratories) and visualized under fluorescence microscopy (Axio Observer Z1, ZEISS). Analysis was performed with CASP.

Protein purification

His-GFP–RBMX fusion protein was expressed using Bac-to-Bac system (Thermo Fisher Scientific) in Sf9 (insect cell line) cells. Cells were harvested and resuspended in lysis buffer (10 mM Tris-HCl, 10 mM NaCl, 20 mM Imidazole). After sonication, the fusion protein was purified by nickel affinity purification.

Electrophoretic mobility shift assay (EMSA)

100 fM biotin-labeled oligonucleotides (5′-(CCCTAA)$_3$GTAGCATCGACG-3′ or 5′-(GGAAT)$_6$-3′) were incubated with 2 μg protein at the room temperature for 20 min in binding buffer (10 mM Tris-HCl (pH 8.0), 10 mM $MgCl_2$, 10 mM NaCl). Then the protein/DNA mixture was separated in 5% (wt/vol) native PAGE gel, transferred to nylon membrane and hybridized with Streptavidin-HRP. The membrane was visualized by ECL developing using a Luminous Imaging System (Tanon).

Microscale thermophoresis (MST)

Increasing concentrations (0nM–25 μM) of oligonucleotides (5′-(CCCTAA)$_3$GTAGCATCGACG-3′) were incubated with 220 nM protein at the room temperature for 20 min in binding buffer (10 mM Tris-HCl (pH 8.0), 10 mM MgCl, 10 mM NaCl). The MST assay was carried out following the protocol provided by manufactory. Overall, 40% of LED power and 40% MST power were used.

Chromatin immunoprecipitaton

293T cells were transfected with either Flag-RBMX or Flag-RPA1 for 48 h and treated with 100 nM CPT for 24 h. Cells were cross-linked by adding formaldehyde directly to culture medium to a final concentration of 1% and incubated for 10 min at 37 °C. Medium was aspirated and cells were washed twice using ice-cold PBS with protease inhibitors. Cells were then scraped and pelleted for 5 min at 2000 rpm at 4 °C. Cell pellet was resuspended in 300 μl of cold RIPA buffer (10 mM Tris-HCl pH 7.5, 1 mM EDTA, 0.1% sodium deoxycholate, 1% NP-40, protease inhibitors). Sonication was performed using the Covaris S220 at peak incident power 175, duty factor 10%, cycle per burst 200 for 8 min. Samples were then centrifuged at 13,000 rpm at 4 °C for 10 min, and supernatant was transferred to tenfold dilution buffer (0.01% SDS, 1.1% Triton X- 100, 1.2 mM EDTA, 16.7 mM Tris-HCl, pH 8.1, 167 mM NaCl). Each sample was incubated with 20 μl flag-beads (Sigma) for 4 h at 4 °C, washed once with low salt wash buffer (0.1% SDS, 1% Triton X-100, 2 mM EDTA, 20 mM Tris-HCl, pH 8.1, 150 mM NaCl), once with high salt wash buffer (0.1% SDS, 1% Triton X-100, 2 mM EDTA, 20 mM Tris-HCl, pH 8.1, 500 mM NaCl) and twice with TE buffer (10 mM Tris pH 8.0, 1 mM EDTA). The protein–DNA complex was eluted twice by adding 250 μl elution buffer (1%SDS, 0.1 M $NaHCO_3$) at the room temperature and rotating for 15 min. Cross-linking was reversed by adding 50 μl 3 M CH_3COONa to the complex and incubating at 65 °C for 4 h. Proteins were then digested with proteinase K at 45 °C for 1 h. DNA was recovered by phenol/chloroform extraction and ethanol precipitation. Samples were sent to Genewiz (Suzhou, China) for sequencing.

ChIP-seq data analysis

ChIP libraries and their respective inputs were sequenced by Genewiz (Suzhou, China), generating 150 bp double-end sequencing reads. Reads were aligned to the hg38 genome using Bowtie2 [28] with default parameters. No more than 2 bp mismatches were allowed for each read. The best scoring alignment per read was kept. Among all aligned reads, ~80% were unique reads. Duplicated reads were removed by samtools. The remaining reads were converted to normalized BigWig files for genomic visualization using Deeptools (version 3.4.1), with reads coverage for each window of 100 bp normalized by CPM (Counts per million mapped reads). MACS2 (version 2.2.4) was used to call peaks between IP and input samples with the parameters '-p 1e-12 –nomodel –nolambda'. All peaks were annotated by HOMER [29] annotatePeaks.pl program. Repetitive DNAs were screened using RepeatMasker [30] online. Motifs were identified using MEME suite [31]. Two biological replicates were performed.

Statistics

GraphPad Prism 7 was used for statistical analysis. Results are shown as mean ± SEM and the unpaired Student's two-tailed *t* test was used to determine the statistical significance (*$P < 0.05$; **$P < 0.01$; ***$P < 0.001$; ****$P < 0.0001$). For every figure, statistical tests are justified as appropriate.

Results

RBMX localizes to the sites adjacent to RPA and is responsible for ATR activation

Stalled replication forks result in activation of ATR, which is characterized by phosphorylation on T1989 of ATR [4, 32]. It is previously reported that RBMX is involved in DDR and maintenance of genome stability; we thus set to explore the possible role of RBMX in ATR activation. Phosphorylated-ATR (ATR pT1989) was examined in both U2OS cells that bear a high level of endogenous DNA replication stress [33–36] and HeLa cells treated with CPT that causes replication fork collapse by inhibiting Topoisomerase I [37]. We observed much less of ATR pT1989 in RBMX depleted cells than that in control cells with no significant change of total ATR (Fig. 1a). RBMX depleted cells also displayed lower levels of phosphorylated CHK1 (CHK1 pS345) and phosphorylated RPA2, which are downstream targets of activated ATR [38] (Fig. 1a; Supplemental Fig. S1A). This RBMX-dependent activation of ATR was also observed in HeLa cells treated with HU or aphidicolin that induces replication fork stalling [39] (Supplemental Fig. S1B). Depletion of RBMX resulted in increased, slightly decreased (5%) or unchanged mRNA level of ATR in U2OS, 293T, or CPT-treated HeLa cells, respectively (Fig. 1b; Supplemental Fig. S1C). Given protein level of ATR remaining unchanged upon depletion of RBMX (Fig. 1a), we concluded that it is unlikely that RBMX promotes ATR activation by upregulating the expression of ATR. Moreover, the expression level of

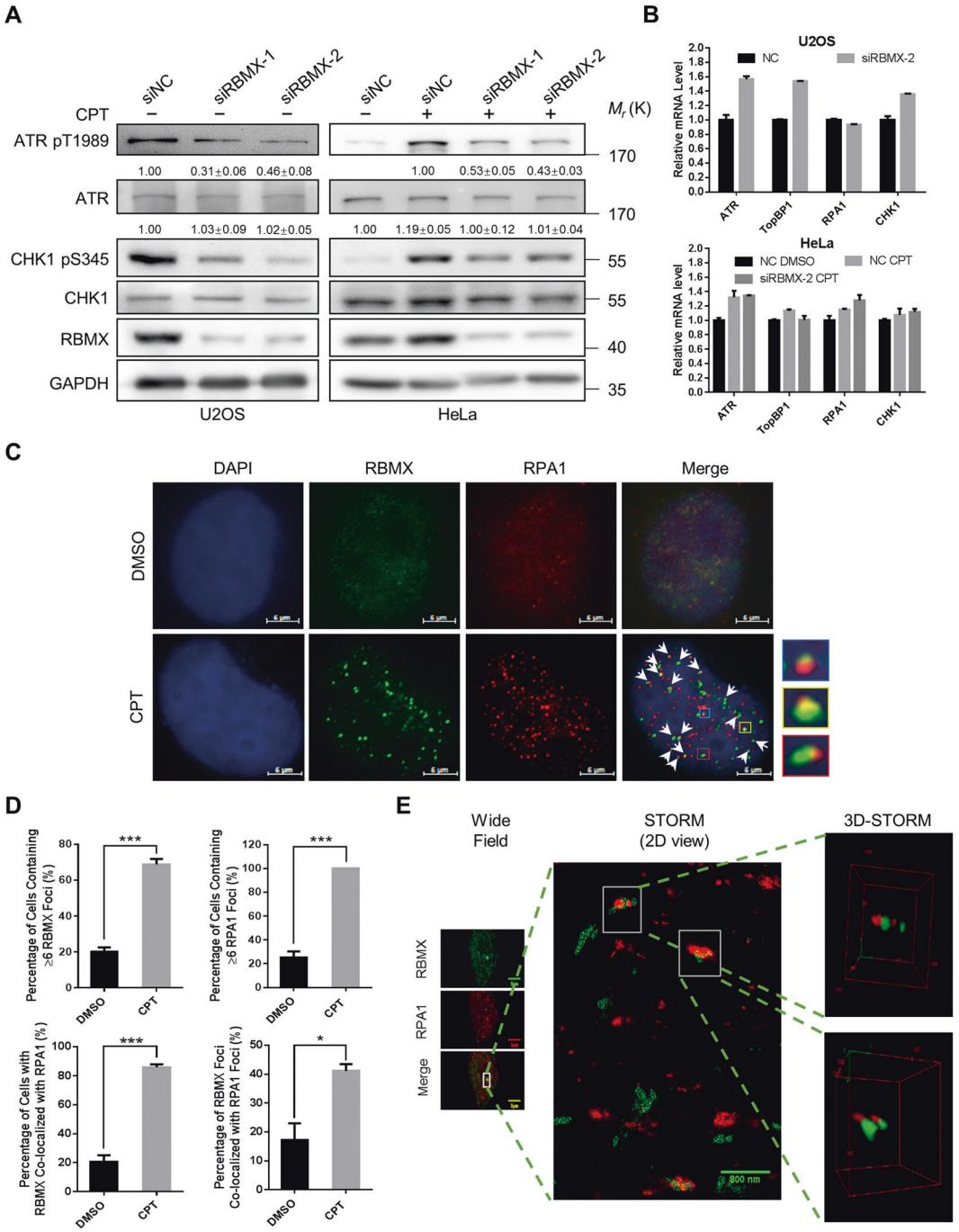

Fig. 1 RBMX localizes to the sites adjacent to RPA and is responsible for ATR activation. a Immunoblot analysis of activated ATR, total ATR, phosphorylated CHK1, and total CHK1 in HeLa or U2OS cells transfected with siNC or siRBMX-1/2. HeLa cells were treated with 100 nM CPT for 24 h prior to analysis. Quantitative values are the mean ± SEM of $n = 3$ experiments. **b** Detection of mRNA levels of ATR, TopBP1, RPA1, and CHK1 in U2OS or HeLa cells transfected with siNC or siRBMX-2. HeLa cells were treated with 100 nM CPT for 24 h during transfection. mRNA levels were quantified by qPCR. **c** Detection of RBMX and RPA1 foci in HeLa cells treated with DMSO or CPT (100 nM). Cells were treated with CPT for 24 h and stained for RBMX and RPA1. Co-localized foci were indicated with arrows. Scale bars, 5 μm. **d** Quantification of **c**. Percentage of RBMX or RPA1 foci positive cells (≥6 foci in cell), percentage of RBMX foci co-localizing with RPA1 foci were calculated. Percentage of RBMX/RPA1 co-localized cells (the cell having at least three RBMX/RPA1 co-localized foci in its nucleus is defined as a "RBMX-RPA co-localized cell"; more than 100 cells were randomly picked up for scoring) were calculated. All values are the mean ± SEM of $n = 3$ experiments. *$P < 0.05$; ***$P < 0.001$. The Student's t test was used to determine the statistical significance. **e** Visualization of RBMX and RPA protein at single molecule level using STORM. RBMX and RPA1 foci were subjected to observation under Wide Field and STROM. Representative 2D and 3D views were shown. Scale bars, 5 μm in Wide Field, 800 nm in STORM (2D view).

TopBP1, RPA1, or CHK1 was either increased or not affected by RBMX depletion.

CPT and etoposide (VP-16) induce ATR-mediated DDR, leading to cell cycle arrest or cell death depending on the doses used [40, 41]. We observed that knockdown of RBMX resulted in vast decrease of cell viability, similar to phenomena when ATR is depleted. In addition, concurrent depletion of RBMX and ATR led to moderate but not significant decrease of cell viability compared with that of depleting ATR alone (Supplemental Fig. S1D). These results support the idea that RBMX and ATR are in the same signal transduction pathway that sensitizes cellular response to replication stress.

RPA interacts with ssDNA and plays an essential role in activation of ATR [42]. RPA-bound ssDNA recruits ATR to DNA damage sites, promoting autophosphorylation of ATR and activation of ATR by TopBP1 at ssDNA–dsDNA junctions [12]. We then examined the relationship between RPA and RBMX. Like RPA, RBMX displayed a diffuse nuclear distribution under a normal circumstance [23, 24], both RBMX and RPA formed punctate foci on chromatin when cells were treated with CPT (Fig. 1c). Strikingly, more than 80% cells showed co-localized RBMX and RPA foci when treated with CPT and up to 40% of RBMX were co-localized with RPA foci in HeLa and U2OS cells (Fig. 1d; Supplemental Fig. S1E, F). However, a close examination of co-localized foci revealed adjacent or partially overlapping RBMX and RPA foci, implying that RBMX and RPA may occupy close but distinct sites on damaged DNA.

Stochastic optical reconstruction microscopy (STORM) at nanometer scale resolution was used to visualize precise location of RBMX and RPA proteins on chromatin [43]. STORM allows collecting a series of images, which allowed 2-dimensional (2D) and 3D views of the two proteins to be reconstructed. In the majority of the 2D views, the space occupied by RBMX (green) did not overlap with the space occupied by RPA (red) (Fig. 1e). In some cases, the RBMX and RPA signals appeared to overlap in the 2D reconstructed images; however, 3D reconstruction revealed that RBMX and RPA are localized to adjacent but non-overlapping sites (Fig. 1e; Supplemental Movies S1, 2). These results suggest that RBMX and RPA do not co-localize precisely on chromatin, and likely make no physical contact with each other, even though they are recruited to same region of DNA damage.

RBMX binds to ssDNA

To confirm the results presented above, the interactions between RBMX and RPA were examined by co-immunoprecipitation (co-IP). Co-IP results showed that RBMX did not co-immunoprecipitate with RPA1 and RPA-interacting protein ATRIP in 293T cells treated with CPT (Fig. 2a), demonstrating no physical interaction between RBMX and RPA. Interestingly, TopBP1, a major activator that is responsible for ATR activation, was co-immunoprecipitated with RBMX (Fig. 2a). The association between RBMX and TopBP1 will be studied in detail below.

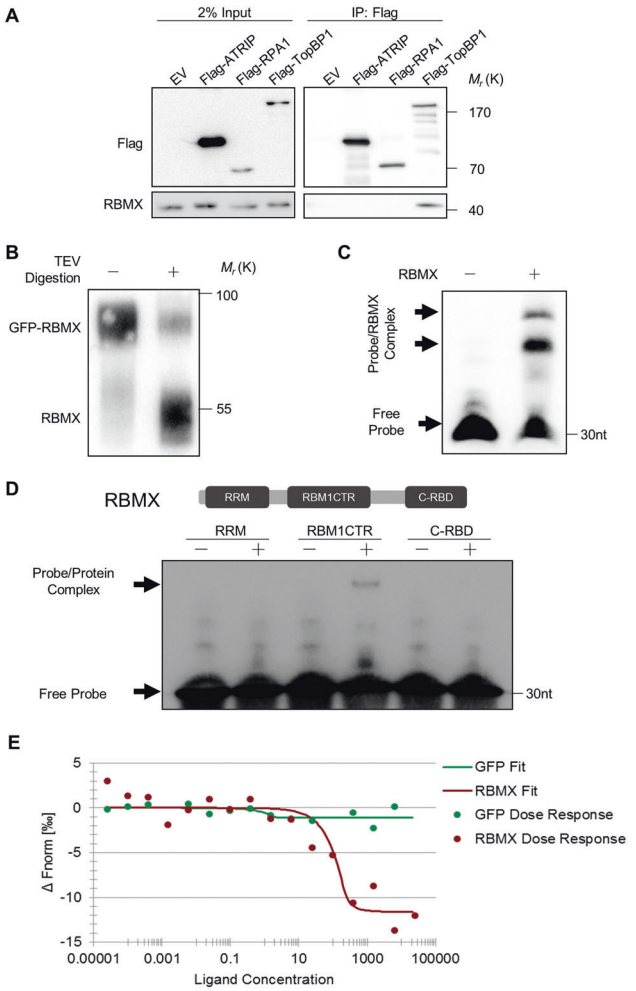

Fig. 2 RBMX binds to ssDNA. a Co-IP assay to determine the interaction of RBMX with ATRIP, RPA1, and TopBP1. Flag-labeled ATRIP, RPA1, and TopBP1 was over-expressed in 293 T cells. Cells were treated with 100 nM CPT for 24 h and immunoprecipitates were immunoblotted with Flag and RBMX antibody, respectively. **b** Immunoblot analysis of GFP–RBMX, RBMX protein purified from insect Sf9 cells. RBMX was obtained by TEV cleavage of GFP–RBMX fusion protein. **c** EMSA showing binding activity of RBMX to ssDNA (5′-(CCCTAA)$_3$GTAGCATCGACG-3′). Shifted bands were indicated by arrows. **d** EMSA determining the ssDNA binding activity of different domains in RBMX. Indicated domains were purified from insect Sf9 cells and assayed. **e** MST assay to determine the binding affinity of RBMX and ssDNA. GFP–RBMX or GFP (control) was incubated with increased concentration of ssDNA (5′-(CCCTAA)$_3$ GTAGCATCGACG-3′) and then subjected to MST. The normalized fluorescence ΔF_{norm} at $t = 20$ s is plotted for different concentrations of ssDNA. The thermophoresis of GFP (green) shows no ssDNA concentration dependence.

Given that RBMX bears RRM (RNA recognition motif) that may also bind to ssDNA, we suspected that RBMX binds to ssDNA itself. To directly test for ssDNA binding activity, a GFP–RBMX fusion protein was expressed and purified from insect Sf9 cells (Fig. 2b), and used in EMSA. The protein was incubated with biotin-labeled telomeric (CCCTAA) or centromeric (GGAAT) oligonucleotides (probes). The result revealed that RBMX altered the mobility of both ssDNA probes, forming one higher and one lower MW protein–ssDNA complex (Fig. 2c; Supplemental Fig. S2A). The slow migrating higher MW species may include an RBMX protein dimer. Similar assays were performed using truncated RBMX fragments including the RRM, RBM1CTR, or C-RBD domain of RBMX (Fig. 2d; Supplemental Fig. S2B). This experiment indicated that ssDNA binding activity is associated with the RBM1CTR domain of RBMX.

The MST assay was performed to measure the binding affinity of RBMX to ssDNA. GFP-fused RBMX was purified and incubated with ssDNA with concentrations ranging from 0 to 25 μM. The binding curve was obtained by plotting the normalized Δfluorescence at $t = 20$ s against ssDNA concentrations (Fig. 2e; Supplemental Fig. S2C). The dissociation constant (K_D) for RBMX binding to ssDNA is ~11 nM (Fig. 2e). This is comparable with the K_D of 10 nM for RPA–ssDNA association, although the value may vary depending on the sequence and binding condition [44–48].

RBMX preferentially associates with repetitive DNAs along with RPA

To characterize the binding sites of RBMX and RPA on chromatin, 293T cells were treated with CPT and binding profiles were obtained by ChIP-seq assay. We first characterized the nature of DNA obtained from RBMX-ChIP. We observed that digestion with single-stranded specific exonuclease ExoI & $RecJ_f$ eliminated almost all precipitated DNA. However, these DNA were resistant to DSN (Duplex Specific Nuclease) digestion. In contrast, DNA precipitated by H2AFY-ChIP, a typical double-stranded DNA binding protein, were sensitive to DSN, but resistant to ExoI & $RecJ_f$ digestion (Supplemental Fig. S2D). This result revealed single-stranded nature of RBMX-associated DNA, suggesting that RBMX binds to ssDNA in vivo, although it did not exclude the possibility that RBMX may bind to ssDNA indirectly through interacting with other DNA binding protein.

RBMX ChIP-seq profile was highly correlated with RPA ChIP-seq profile, both showing strong peaks at centromeres (Fig. 3a, b). Among identified peaks of RBMX, 47.8% were shared with RPA (the peak of RBMX having at least 90% identity with RPA peak is considered as a shared peak), suggesting that RBMX and RPA bind to the same or adjacent sites on genome (Fig. 3c). Moreover, analysis of RBMX reads revealed enrichment of a purine-rich motif (GAATGGAATGGA) (Fig. 3d). In contrast, RPA-bound sequences displayed an enriched pyrimidine-rich motif (ATGATTCCATTC) (Fig. 3d), which is consistent with previous consensus that RPA binds to ssDNA with a high preference for pyrimidines [46]. Interestingly, the two motifs are reversely complementary in sequence, raising the intriguing possibility that RBMX and RPA bind to each strand of dsDNA, respectively.

To characterize the DNA sequences bound by both RBMX and RPA, we annotated their shared peaks. The results showed that these sequences are mostly enriched on repetitive DNAs including rRNA, simple repeats and satellite DNAs (Fig. 3e). More specifically, by screening the sequences in database of repetitive DNAs using RepeatMasker [30], we found that ~70% sequences belong to repetitive DNAs, in which ~80% are satellite DNAs and ~20% are simple repeats (microsatellite DNAs) (Fig. 3f). Thus, we concluded that RBMX is preferentially localized to repetitive DNAs, where replication is challenged [49].

RBMX interacts with TopBP1

Interaction between RBMX and TopBP1 was detected by co-IP assay using antibody targeting endogenous TopBP1 in both 293T and HeLa cells (Supplemental Fig. S3A, B). Reverse co-IP using GFP–RBMX to pull down TopBP1 confirmed the interaction between the two proteins in 293T cells (Supplemental Fig. S3C). In addition, we observed that much more RBMX was pulled-down by TopBP1 from cells treated with CPT compared with untreated cells, indicating that the interaction between RBMX and TopBP1 is largely dependent on genotoxic stress (Supplemental Fig. S3C, D). Furthermore, when samples were pre-treated with RNase A or DNase I prior to IP, we observed no change of RBMX precipitated by TopBP1, suggesting that RBMX and TopBP1 interaction is not mediated by DNA or RNA (Supplemental Fig. S3E).

Under normal circumstances, TopBP1 localized to the nucleolus [50] (Supplemental Fig. S3F). However, in cells treated with CPT, TopBP1 moved out of nucleolus and was detected in nuclear foci that was co-localized with RBMX (Fig. 4a, b; Supplemental Fig. S3G, H). Moreover, high resolution 2D and 3D STORM demonstrated that RBMX and TopBP1 co-localize at a single molecular level, which is consistent with a direct interaction between RBMX and TopBP1 (Fig. 4c; Supplemental Movies S3, 4).

To study this interaction in detail, we constructed truncated proteins of both RBMX and TopBP1. Co-IP studies in cells expressing GFP-labeled fragments of RBMX corresponding to the RRM, RBM1CTR, or the C-RBD [19, 23]

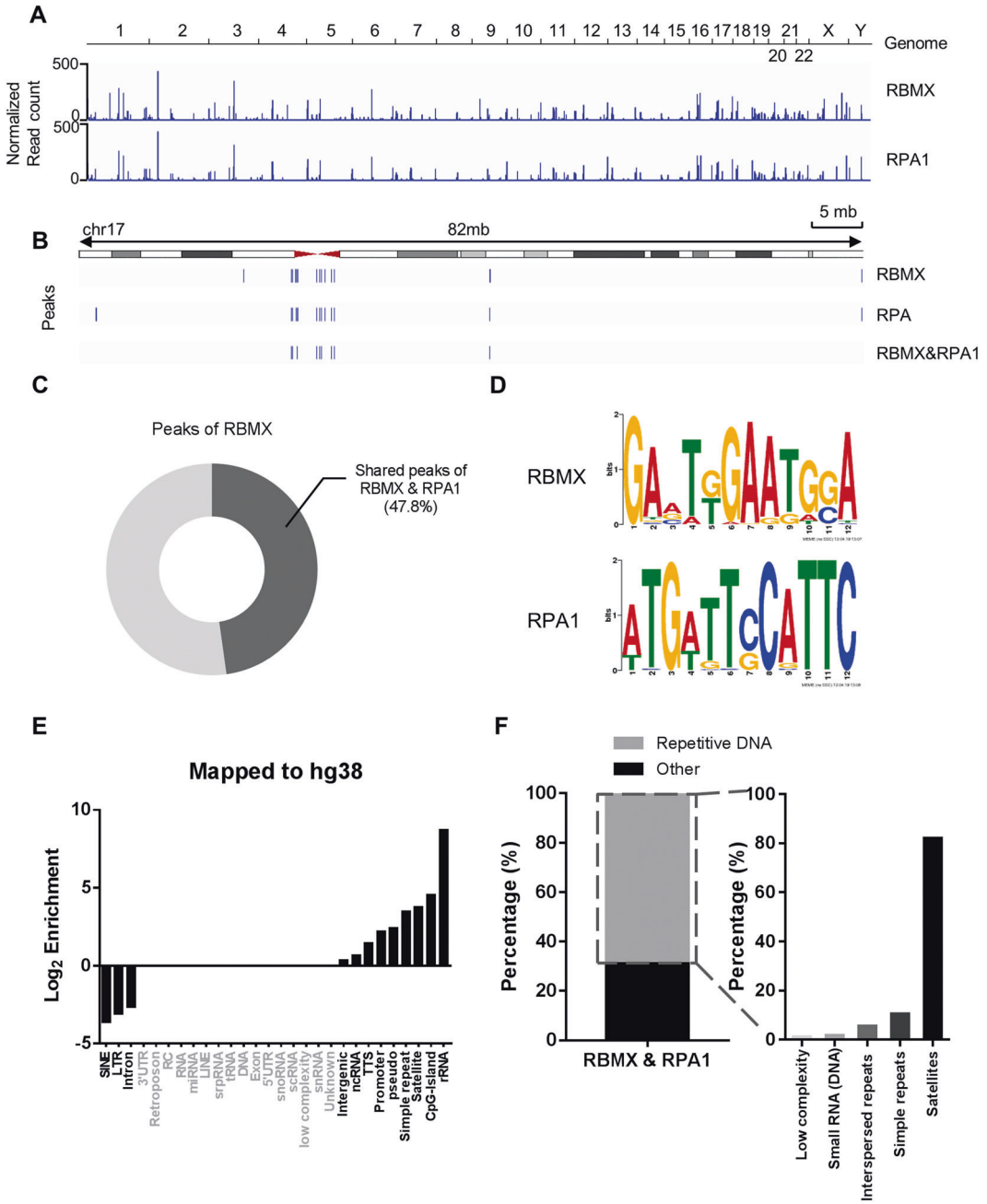

Fig. 3 RBMX preferentially associates with repetitive DNAs together with RPA. a Coverage tracks of reads of RBMX ChIP-seq and RPA ChIP-seq. 293T cells were transfected with either Flag-RBMX or Flag-RPA1 and treated with 100 nM CPT for 24 h. Protein–DNA complex was pulled-down using Flag-beads and recovered DNA was sequenced. **b** Representative peaks of RBMX and RPA1 over input. Shared peaks were RBMX peaks that have at least 90% identity with RPA peaks. Chromosome 17 is shown as an example. **c** The percentage of shared peaks of RBMX and RPA in peaks of RBMX. **d** Logo of motifs identified by MEME (Multiple Em for Motif Elicitation) in ChIP-seq peaks of RBMX or RPA1. **e** Annotation of the shared peaks of RBMX and RPA. Elements with no peaks are grayed out. **f** The percentage of shared peaks of that belong to repetitive DNA (left panel). Shared peak sequences were screened and analyzed by RepeatMasker. Types of repetitive DNAs and their percentages were shown in right panel.

domains, respectively, showed that RBM1CTR and C-RBD fragments co-immunoprecipitate with Flag-TopBP1, while the RRM fragment of RBMX did not co-immunoprecipitate Flag-TopBP1 (Fig. 4d, e). Conversely, Flag-tagged truncated TopBP1 Δ1–2 and Δ7–8, but not Δ1–5, co-immunoprecipitated with RBMX, suggesting that BRCT domains (3, 4, and 5) of TopBP1 is responsible for interaction with RBMX (Fig. 4f, g).

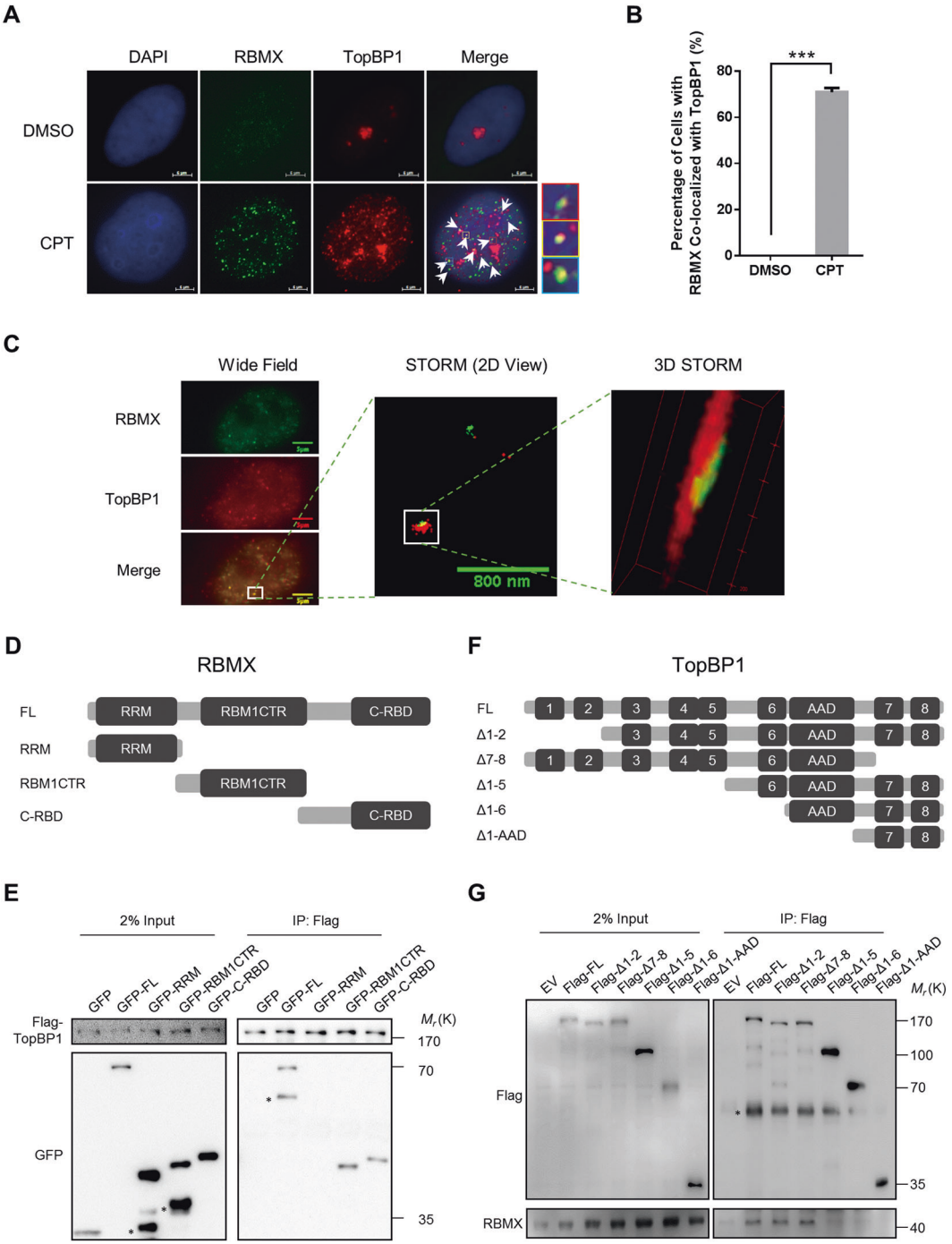

Fig. 4 RBMX interacts with TopBP1. a Immunofluorescence (IF) assay to detect the co-localization of RBMX and TopBP1. HeLa cells were treated with DMSO or 100 nM CPT for 24 h and stained using antibody against RBMX and TopBP1. Scale bars, 5 μm. **b** Quantification of **a**. Percentage of cells with co-localized RBMX/TopBP1 foci was determined. Error bars are SEM from $n = 3$ experiments; Student's, two-tailed, unpaired t test. ***$P < 0.001$. **c** Visualization of RBMX and TopBP1 protein using STORM. RBMX and TopBP1 foci were observed under Wide Field and STORM. 2D and representative 3D views were shown. Scale bars, 5 μm in Wide Field, 800 nm in STORM (2D view). **d** Schematic diagram showing the domains of RBMX. **e** Co-IP assay to determine the domain of RBMX that interacts with TopBP1. 293T cells transfected with Flag-TopBP1 and GFP-tagged RBMX and its domain (RRM, RBM1CTR, and C-RBD) were treated with 100 nM CPT for 24 h and subjected to immunoprecipitation with Flag-beads. Immunoprecipitates were immunoblotted with Flag and GFP antibodies, respectively. **f** Schematic diagram showing the domains of TopBP1. **g** Co-IP assay to determine the domain of TopBP1 that interacts with RBMX. 293T cells transfected with Flag-tagged TopBP1 and its truncated proteins were treated with 100 nM CPT for 24 h and subjected to immunoprecipitation with Flag-beads. Immunoprecipitates were immunoblotted with Flag and RBMX antibodies, respectively.

Interaction of RBMX with TopBP1 is independent of 9-1-1 complex

As expected, depletion of RBMX reduced the amount of phosphorylated-ATR (p-ATR) in CPT-treated cells, while ectopic expression of RBMX rescued p-ATR to its normal level (Supplemental Fig. S4A). In contrast, when TopBP1 was knocked down along with RBMX, ectopic expression of RBMX did not rescue p-ATR to its normal level (Supplemental Fig. S4B). This indicated that RBMX-mediated activation of ATR depends on TopBP1.

In the prevailing model for ATR activation, TopBP1 is recruited to an ssDNA–dsDNA junction by 9-1-1 complex [51–53], TopBP1 then allosterically activates ATR recruited by RPA. To investigate whether RBMX functions together with 9-1-1 complex, co-IP assays were performed with RBMX and Rad9A or Rad17, two proteins that are required to recruit TopBP1 to an ssDNA–dsDNA junction [51–53]. The results showed that neither Rad17 nor Rad9A co-immunoprecipitate with RBMX (Fig. 5a, b). One interpretation of these data is that RBMX and the 9-1-1 complex interact with TopBP1 independently, acting at different sites. Consistent with this idea, RBMX and TopBP1 interaction was not affected by knockdown of Rad17, Rad9A, or RPA (Fig. 5c; Supplemental Fig. S4C).

Next, we explored whether RBMX/TopBP1 and 9-1-1/TopBP1 participate in distinct pathways for activating ATR. First, the depletion of RBMX or Rad9A or Rad17 only partially decreased the total number of nuclear TopBP1 foci in cells treated with CPT (Fig. 5d, e). The amount of TopBP1 (intensity) in nucleolus increased, accordingly (Fig. 5d, e; Supplemental Fig. S4D). However, upon depletion of RBMX and Rad9A, or RBMX and Rad17, nuclear TopBP1 foci were nearly completely eliminated, and the amount of TopBP1 in nucleolus was back to the equal level as that in cells without CPT treatment (Fig. 5d, e; Supplemental Fig. S4D). These results are consistent with the idea proposed above that RBMX and the 9-1-1 complex facilitate positioning of TopBP1 to chromatin independently, acting in two distinct pathways. Second, depletion of RBMX, Rad9A, or Rad17 reduced p-ATR in CPT-treated cells by ~40% (Fig. 5f, g), while depletion of RBMX and Rad17, RBMX and Rad9A, or depletion of only TopBP1 reduced p-ATR by ~80% (Fig. 5f, g; Supplemental Fig. S4E, F). In contrast, simultaneous depletion of Rad17 and Rad9A reduced p-ATR by ~40% (Fig. 5f, g). These data supported the idea that RBMX and 9-1-1 act in two distinct pathways to activate ATR, both of which are TopBP1-dependent.

RBMX deficiency leads to genome instability

Because activation of ATR is an essential step for cells to resolve the replication stress, we predicted that a defect in or depletion of RBMX will impair the cellular response to replication stress, which may lead to persistent activation of DDR and genome instability. Consistent with this prediction, depletion of RBMX in HeLa and U2OS cells increased the percentage of PCNA-positive cells, indicating stressed DNA replication in these cells [54] (Supplemental Fig. S5A–C). Interestingly, cell cycle analysis by FACS showed only slight increase of S and G2/M phase cells in response to depletion of RBMX (Supplemental Fig. S5D, E). Also, analysis of in situ pattern of PCNA staining demonstrated not significant increase of S phase cells, but remarkable increase of non-S phase cells that bear damaged DNA (Supplemental Fig. S5F) [55]. These results indicated that RBMX deficiency may lead to stressed replication forks during S phase, and accumulation of DNA damage in non-S phase cells, both requiring the activation of ATR.

Moreover, DDR, which is marked by 53BP1 foci on genome, accumulated in RBMX depleted HeLa and U2OS cells (Supplemental Fig. S6A–D). Consistently, more DNA fragments were detected by comet assay in RBMX-deficient cells (Fig. 6a, b). Depletion of RBMX also increased the frequency of sister chromatid exchanges (SCE) (a marker of genotoxicity [56]) (Fig. 6c, d; Supplemental Fig. S6E, F) and the occurrence of micronuclei, indicating the activation of genome instability due to defective DNA replication [57] (Fig. 6e, f; Supplemental Fig. S6G, H). These results demonstrate that RBMX plays an essential role in the cellular response to DNA replication stress and in maintaining genome stability.

Discussion

Role of RBMX in activation of ATR

In the prevailing model for activation of ATR, ATR is positioned to RPA-coated ssDNA and subsequently activated by TopBP1 that is recruited to ssDNA–dsDNA junctions by 9-1-1 complex [12, 51–53]. This study uncovers a new RBMX-dependent but 9-1-1 complex-independent manner for activation of ATR (Fig. 6g). In this model, TopBP1 is enabled to activate ATR in concert with RBMX in the absence of an ssDNA–dsDNA junction or 9-1-1 complex. We propose that RBMX/TopBP1 and 9-1-1/TopBP1 operate independently and simultaneously, such that ATR is fully activated in response to replication stress. Previous study discovered that RBMX promotes homologous recombination-mediated DNA damage repair by upregulating the expression of BRCA2 [23]. This and our finding are not mutually exclusive, giving that RBMX may have distinct functions in response to DNA damage or replication stress, respectively. Here, we provided the evidences demonstrating that RBMX directly participates in

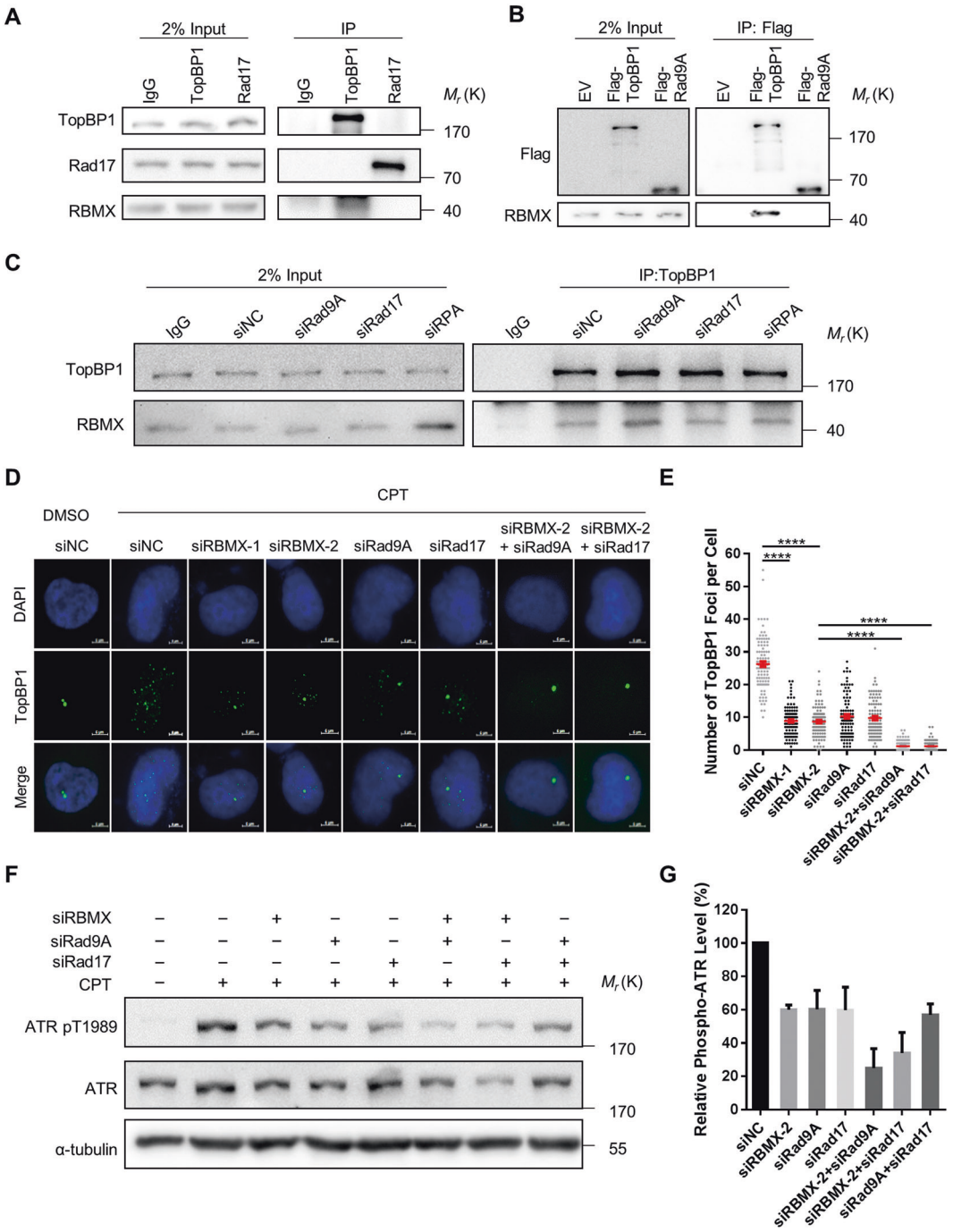

Fig. 5 Interaction of RBMX with TopBP1 is independent of 9-1-1 complex. a Co-IP assay to determine the interaction of endogenous RBMX with Rad17 in 293T cells. Cells were treated with 100 nM CPT for 24 h and immunoprecipitated with TopBP1 or Rad17 antibodies, respectively. IgG was used as a negative control. Immunoprecipitates were immunoblotted with indicated antibodies. **b** Co-IP assay to determine the interaction of endogenous RBMX with Rad9 in 293T cells. Cells were transfected with Flag-TopBP1, Flag-Rad9A, or EV and treated with 100 nM CPT for 24 h. Cell lysates were used for immunoprecipitation with Flag-beads. Immunoprecipitates were immunoblotted with Flag and RBMX antibody, respectively. **c** Co-IP assay showing the interaction of RBMX and TopBP1 is independent of Rad17, Rad9A, and RPA in 293T cells. 293T cells transfected with indicated siRNAs were treated with CPT for 24 h and subjected to immunoprecipitation using TopBP1 antibodies. IgG was used as a negative control. **d** Immunofluorescence (IF) detection of TopBP1 migrating from nucleoli to nuclei in response to CPT treatment. HeLa cells were transfected with indicated siRNAs and stained for TopBP1. Scale bars, 5 μm. **e** Quantification of **d**. The number of TopBP1 foci excluding foci in nucleoli was determined. $n = 100$ cells were analyzed. Error bars are SEM; Student's, two-tailed, unpaired t test. $^{****}P < 0.0001$. **f** Immunoblot analysis of activated ATR in HeLa cells transfected with indicated siRNAs. Cells were treated with 100 nM CPT for 24 h prior to analysis. **g** Quantification of relative level of activated ATR. Data were from three independent experiments.

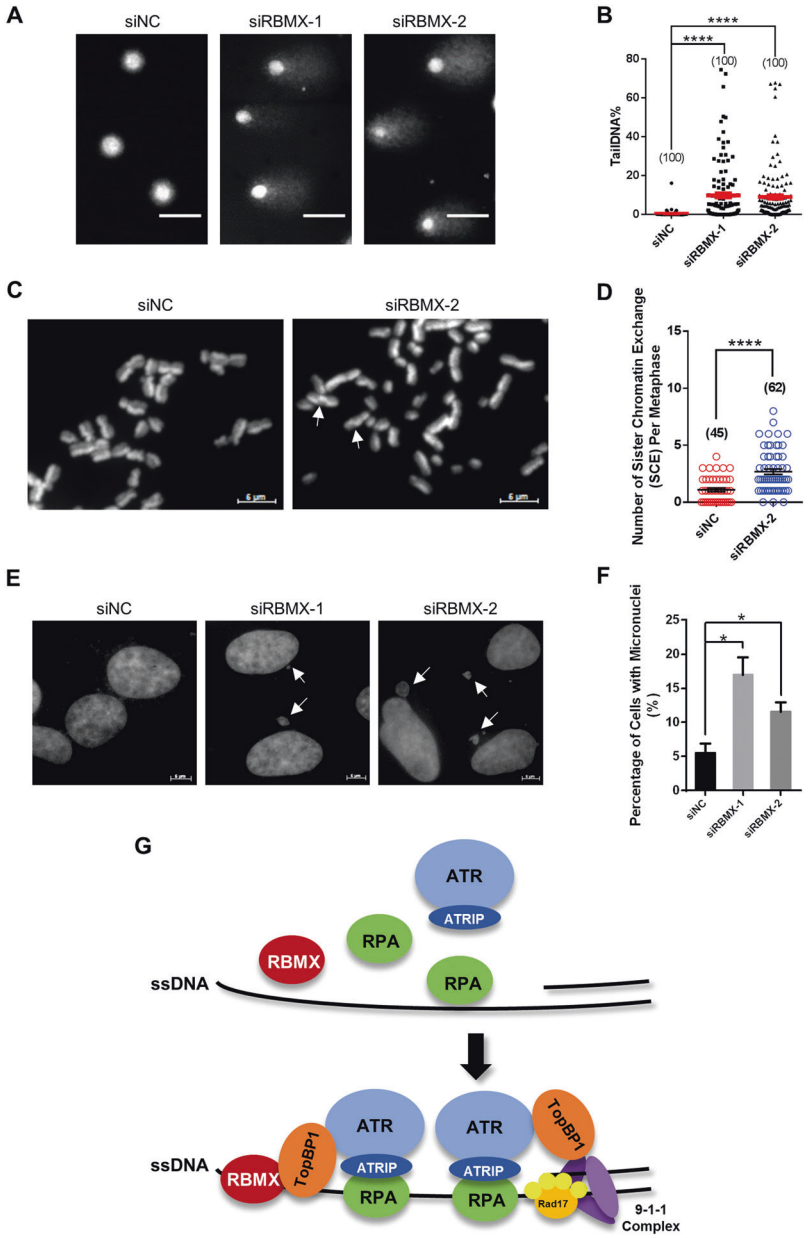

Fig. 6 RBMX deficiency leads to genome instability. a Comet assay detection of DNA fragments in normal and RBMX-deficient HeLa cells. Scale bars, 100 μm. **b** Quantification of **a**. $n = 100$ cells were analyzed in each group. Error bars are SEM; Student's, two-tailed, unpaired t test. $^{****}P < 0.0001$. **c** Representative image showing sister-chromatin exchanges (SCEs) in normal and RBMX-deficient HeLa cells. Scale bars, 5 μm. **d** Quantification of **a**. The number of metaphases analyzed (n value) is indicated. Error bars are SEM. The Student's t test was used to determine the statistical significance. $^{****}P < 0.0001$. **e** Observation of micronuclei in normal and RBMX-deficient HeLa cells. Scale bars, 5 μm. **f** Quantification of **e**. Error bars are SEM from three independent experiments; Student's, two-tailed, unpaired t test. $^{*}P < 0.05$. **g** Working model for ATR activation by RBMX/TopBP1 mediated manner. RBMX binds to ssDNA and interacts with TopBP1 at the place next to RPA. Since ATR is recruited by RPA through interacting with ATRIP, nearby TopBP1 acts to activate ATR. This is independent of 9-1-1/TopBP1 mediated activation of ATR that occurs at ssDNA–dsDNA junction site.

activation of ATR by associating with both ssDNA and TopBP1 in response to replication stress. This model, however, does not exclude the possibility that TopBP1 directly binds to ssDNA [58]. RBMX/TopBP1 interaction thus facilitates positioning of TopBP1 to the place where activation of ATR is needed.

RBMX binds to ssDNA adjacent to RPA

Our results showed that RBMX binds to ssDNA with the affinity similar to RPA (Fig. 2) [44]. While RBMX and RPA are co-localized under normal fluorescence microscope, no interaction between RBMX and RPA1 was detected in co-IP assay. The observation of RBMX and RPA under STORM confirmed nonoverlapping between these two proteins. These results suggest that RBMX and RPA may bind to distinct but adjacent sites of ssDNA on genome.

Using ChIP-seq, we obtained the binding profile of RBMX and RPA on genome in response to replication stress. Interestingly, 47.8% binding sites of RBMX were highly overlapped with RPA, suggesting that two proteins may bind to the same sites of genome, specifically, adjacent sequences in ssDNA of stalled replication fork (Fig. 3c). Overall, 60% RBMX that do not co-localize with RPA may function to regulate the transcription of DNA damage repair-related genes [23] or to form NARC1 complex (NORAD-activated ribonucleoprotein complex 1) to

suppress genome instability, as proposed previously [25]. In addition, among RBMX and RPA overlapped sequences, we identified a number of fragile sites that are highly susceptible to breakage upon replication stress (Supplemental Table S1), implying a potential role of RBMX and RPA to prevent the fragility of such locus [59, 60].

Analysis of ChIP-seq data had also identified preferential binding motifs for RBMX and RPA. We found that whereas RPA displays a high preference for pyrimidine-rich sequence, as previously reported [46], RBMX preferentially binds to purine-rich sequence. To our surprise, the primary binding motif for RBMX is reversely complementary to that for RPA. The easiest interpretation is that RBMX and RPA bind to two strands of replication fork, respectively. In this scenario, RBMX and RPA are localized to relatively close sites within replication fork, enabling the activation of ATR by TopBP1. It should be noted that previous RPA ChIP-seq experiments performed by Barlow et al. showed that RPA are localized to highly transcriptional gene locus at early S phase [59], which have been termed as early replicating fragile sites. In contrast, mostly repetitive sequences are identified in this study that represent fragile sites induced by CPT throughout S phase during replication.

TopBP1-dependent and 9-1-1-independent activation of ATR by RBMX

Following evidences support that RBMX/TopBP1 act independently of 9-1-1/TopBP1 pathway in activation of ATR: (1) RBMX binds to ssDNA with no requirement of ssDNA–dsDNA junction; (2) Co-IP data show that RBMX does not interact with Rad9A or Rad17, while it interacts specifically with TopBP1 in wild-type extracts and in extracts depleted of Rad9A or Rad17; (3) the effect of RBMX and Rad9A (or Rad17) on mobilization of TopBP1 from the nucleolus to nuclear sites is additive, suggesting that RBMX and Rad9A (or Rad17) function to promote positioning of TopBP1 to damage sites in two distinct pathways; (4) depletion of RBMX or Rad9A (or Rad17) decreases activation of ATR by ~40%, whereas depletion of RBMX and Rad9A decrease activation of ATR by ~80%, indicating that RBMX and Rad9A/Rad17 act in two distinct pathways to activate ATR. Thus, RBMX and 9-1-1 complex participate in two independent pathways for activating ATR, each of which appears to play an equally significant role.

RBMX preferentially binds to repetitive DNAs along with RPA

It is worth noting that only ~40% of RBMX foci are co-localized with RPA in cells challenged by replication stress (Fig. 1c, d). Moreover, analysis of ChIP-seq data revealed that 47.8% of RBMX binding peaks are shared with RPA (Fig. 3c). These results raise the possibility that RBMX is recruited to specific locus on genome where DNA replication is challenged and full activation of ATR is demanded. Indeed, annotation of the shared peaks revealed that these sequences are mostly enriched on locus with repetitive sequences such as rDNAs, satellite DNAs and simple repeats (microsatellite) [61] (Fig. 3e).

Precise duplication of repetitive DNAs is challenged by the fact that repeats are prone to form secondary structures such as hairpins, triplexes, G-quadruplexes, i-motifs, DNA:RNA hybrids (R-loops) and slipped DNA structures [62], which may result in replication fork stalling or in extreme cases replication fork collapse [49]. Recently, it has been reported that repetitive DNAs are principal sites of fork collapse and successful replication of them is highly dependent on ATR [63]. We thus propose that as the initial and critical step, activation of ATR by ssDNA-RBMX-TopBP1 is indispensable to ensure the duplication of repetitive DNAs on genome.

RBMX as a potential target for cancer therapeutics

Rapidly proliferating cells experience high replication stress, and typically activate ATR–CHK1 to ensure successful completion of DNA replication [64]. The incidence of mutation in ATR is extremely low in cancer cells [65]. In addition, ATR-Seckel mice do not develop spontaneous tumors, demonstrating the requirement of ATR for tumorigenesis [9]. In fact, it is reported that a low level of ATR prevents the onset of certain tumors [66, 67]. Therefore, agents that inhibit ATR are promising anticancer drugs, and some ATR inhibitors are currently in clinical trials [68, 69]. RBMX is upregulated in 21 out of 31 cancers tested, and the incidence of mutations in RBMX ranges from 6 to 0% in all cancers with total alteration frequency of 2%. This value is lower than many other genes involved in DDR such as ATM (6%), ATR (5%), and BRCA1 (3%) (Supplemental Fig. S7A, B) [65, 70–72]. These studies suggest that RBMX may also be a promising target for cancer therapeutics. Further investigation is needed to explore this possibility.

Data availability

The raw ChIP-Seq data of RBMX and RPA1 have been submitted to GEO database. The GEO accession number is GSE134980.

Acknowledgements We thank all the members in Zhao's laboratory for insightful scientific discussion. We thank Dr. Zhou Songyang at the School of Life Sciences, Sun Yat-sen University for providing plasmids of Bac-to-Bac system and Dr. Wenqing Zhang for providing Sf9 cells.

Funding This work was supported by National Natural Science Foundation of China Grants [31970683, 81771506]; National Key R&D Program of China [2018YFA0107000]; Guangzhou Municipal People's Livelihood Science and Technology Plan [201803010108].

Author contributions TZ performed most of the experiments. HZ performed protein purification and EMSA experiments. XL performed the STORM experiments. YY, DP, YZ, and JR analyzed the ChIP-seq data. TZ and YZ wrote the paper. TZ, HL, and YZ designed the experiments. YZ supervised the project.

Compliance with ethical standards

Conflict of interest The authors declare that they have no conflict of interest.

Publisher's note Springer Nature remains neutral with regard to jurisdictional claims in published maps and institutional affiliations.

References

1. Liu S, Opiyo SO, Manthey K, Glanzer JG, Ashley AK, Amerin C, et al. Distinct roles for DNA-PK, ATM and ATR in RPA phosphorylation and checkpoint activation in response to replication stress. Nucleic Acids Res. 2012;40:10780–94.
2. Branzei D, Foiani M. The checkpoint response to replication stress. DNA Repair. 2009;8:1038–46.
3. Ciccia A, Elledge SJ. The DNA damage response: making it safe to play with knives. Mol Cell. 2010;40:179–204.
4. Blackford AN, Jackson SP. ATM, ATR, and DNA-PK: the trinity at the heart of the DNA damage response. Mol Cell. 2017;66:801–17.
5. Marechal A, Zou L. DNA damage sensing by the ATM and ATR kinases. Cold Spring Harb Perspect Biol. 2013;5:a012716.
6. Nyberg KA, Michelson RJ, Putnam CW, Weinert TA. Toward maintaining the genome: DNA damage and replication checkpoints. Annu Rev Genet. 2002;36:617–56.
7. Shechter D, Costanzo V, Gautier J. Regulation of DNA replication by ATR: signaling in response to DNA intermediates. DNA Repair. 2004;3:901–8.
8. Brown EJ, Baltimore D. ATR disruption leads to chromosomal fragmentation and early embryonic lethality. Genes Dev. 2000; 14:397–402.
9. Murga M, Bunting S, Montana MF, Soria R, Mulero F, Canamero M, et al. A mouse model of ATR-Seckel shows embryonic replicative stress and accelerated aging. Nat Genet. 2009;41:891–8.
10. Fang Y, Tsao CC, Goodman BK, Furumai R, Tirado CA, Abraham RT, et al. ATR functions as a gene dosage-dependent tumor suppressor on a mismatch repair-deficient background. EMBO J. 2004;23:3164–74.
11. Cortez D, Guntuku S, Qin J, Elledge SJ. ATR and ATRIP: partners in checkpoint signaling. Science. 2001;294:1713–6.
12. Liu S, Shiotani B, Lahiri M, Maréchal A, Tse A, Leung CC, et al. ATR autophosphorylation as a molecular switch for checkpoint activation. Mol Cell. 2011;43:192–202.
13. Kumagai A, Lee J, Yoo HY, Dunphy WG. TopBP1 activates the ATR-ATRIP complex. Cell. 2006;124:943–55.
14. Saldivar JC, Cortez D, Cimprich KA. The essential kinase ATR: ensuring faithful duplication of a challenging genome. Nat Rev Mol Cell Biol. 2017;18:622–36.
15. Haahr P, Hoffmann S, Tollenaere MA, Ho T, Toledo LI, Mann M, et al. Activation of the ATR kinase by the RPA-binding protein ETAA1. Nat Cell Biol. 2016;18:1196–207.
16. Bass TE, Luzwick JW, Kavanaugh G, Carroll C, Dungrawala H, Glick GG, et al. ETAA1 acts at stalled replication forks to maintain genome integrity. Nat Cell Biol. 2016;18:1185–95.
17. Bass TE, Cortez D. Quantitative phosphoproteomics reveals mitotic function of the ATR activator ETAA1. J Cell Biol. 2019;218:1235–49.
18. Soulard M, Della Valle V, Siomi MC, Pinol-Roma S, Codogno P, Bauvy C, et al. hnRNP G: sequence and characterization of a glycosylated RNA-binding protein. Nucleic Acids Res. 1993;21:4210–7.
19. Kanhoush R, Beenders B, Perrin C, Moreau J, Bellini M, Penrad-Mobayed M. Novel domains in the hnRNP G/RBMX protein with distinct roles in RNA binding and targeting nascent transcripts. Nucleus. 2010;1:109–22.
20. Takemoto T, Nishio Y, Sekine O, Ikeuchi C, Nagai Y, Maeno Y, et al. RBMX is a novel hepatic transcriptional regulator of SREBP-1c gene response to high-fructose diet. FEBS Lett. 2007;581:218–22.
21. Moursy A, Allain FH, Clery A. Characterization of the RNA recognition mode of hnRNP G extends its role in SMN2 splicing regulation. Nucleic Acids Res. 2014;42:6659–72.
22. Heinrich B, Zhang Z, Raitskin O, Hiller M, Benderska N, Hartmann AM, et al. Heterogeneous nuclear ribonucleoprotein G regulates splice site selection by binding to CC(A/C)-rich regions in pre-mRNA. J Biol Chem. 2009;284:14303–15.
23. Adamson B, Smogorzewska A, Sigoillot FD, King RW, Elledge SJ. A genome-wide homologous recombination screen identifies the RNA-binding protein RBMX as a component of the DNA-damage response. Nat Cell Biol. 2012;14:318–28.
24. Matsunaga S, Takata H, Morimoto A, Hayashihara K, Higashi T, Akatsuchi K, et al. RBMX: a regulator for maintenance and centromeric protection of sister chromatid cohesion. Cell Rep. 2012;1:299–308.
25. Munschauer M, Nguyen CT, Sirokman K, Hartigan CR, Hogstrom L, Engreitz JM, et al. The NORAD lncRNA assembles a topoisomerase complex critical for genome stability. Nature. 2018;561:132–6.
26. Zhao T, Wang Y, Zhai Y, Qu X, Cheng A, Du S, et al. A user-friendly two-color super-resolution localization microscope. Opt Express. 2015;23:1879–87.
27. Livak KJ, Schmittgen TD. Analysis of relative gene expression data using real-time quantitative PCR and the 2(-Delta Delta C(T)) Method. Methods. 2001;25:402–8.
28. Langmead B, Salzberg SL. Fast gapped-read alignment with Bowtie 2. Nat Methods. 2012;9:357–9.
29. Heinz S, Benner C, Spann N, Bertolino E, Lin YC, Laslo P, et al. Simple combinations of lineage-determining transcription factors prime cis-regulatory elements required for macrophage and B cell identities. Mol Cell. 2010;38:576–89.
30. Smit AFA, Hubley R, Green, P. RepeatMasker. http://repeatmasker.org.
31. Bailey TL, Boden M, Buske FA, Frith M, Grant CE, Clementi L, et al. MEME SUITE: tools for motif discovery and searching. Nucleic Acids Res. 2009;37:W202–8.
32. Nam EA, Zhao R, Glick GG, Bansbach CE, Friedman DB, Cortez D. Thr-1989 phosphorylation is a marker of active ataxia telangiectasia-mutated and Rad3-related (ATR) kinase. J Biol Chem. 2011;286:28707–14.
33. Sobinoff AP, Pickett HA. Alternative lengthening of telomeres: DNA repair pathways converge. Trends Genet: TIG. 2017;33:921–32.
34. Ge Y, Wu S, Zhang Z, Li X, Li F, Yan S, et al. Inhibition of p53 and/or AKT as a new therapeutic approach specifically targeting ALT cancers. Protein Cell. 2019;10:808–24.
35. Min J, Wright WE, Shay JW. Alternative lengthening of telomeres mediated by mitotic DNA synthesis engages break-induced replication processes. Mol Cell Biol. 2017;37:e00226–17.
36. Clynes D, Jelinska C, Xella B, Ayyub H, Scott C, Mitson M, et al. Suppression of the alternative lengthening of telomere pathway by

the chromatin remodelling factor ATRX. Nat Commun. 2015; 6:7538.
37. Berniak K, Rybak P, Bernas T, Zarebski M, Biela E, Zhao H, et al. Relationship between DNA damage response, initiated by camptothecin or oxidative stress, and DNA replication, analyzed by quantitative 3D image analysis. Cytom A. 2013; 83:913–24.
38. Lopez-Girona A, Tanaka K, Chen XB, Baber BA, McGowan CH, Russell P. Serine-345 is required for Rad3-dependent phosphorylation and function of checkpoint kinase Chk1 in fission yeast. Proc Natl Acad Sci USA. 2001;98:11289–94.
39. Koundrioukoff S, Carignon S, Techer H, Letessier A, Brison O, Debatisse M. Stepwise activation of the ATR signaling pathway upon increasing replication stress impacts fragile site integrity. PLoS Genet. 2013;9:e1003643.
40. Pommier Y, Leo E, Zhang H, Marchand C. DNA topoisomerases and their poisoning by anticancer and antibacterial drugs. Chem Biol. 2010;17:421–33.
41. Ulukan H, Swaan PW. Camptothecins: a review of their chemotherapeutic potential. Drugs. 2002;62:2039–57.
42. Marechal A, Zou L. RPA-coated single-stranded DNA as a platform for post-translational modifications in the DNA damage response. Cell Res. 2015;25:9–23.
43. Rust MJ, Bates M, Zhuang X. Sub-diffraction-limit imaging by stochastic optical reconstruction microscopy (STORM). Nat Methods. 2006;3:793–5.
44. Zou Y, Liu Y, Wu X, Shell SM. Functions of human replication protein A (RPA): from DNA replication to DNA damage and stress responses. J Cell Physiol. 2006;208:267–73.
45. Iftode C, Daniely Y, Borowiec JA. Replication protein A (RPA): the eukaryotic SSB. Crit Rev Biochem Mol Biol. 1999;34:141–80.
46. Kim C, Snyder RO, Wold MS. Binding properties of replication protein A from human and yeast cells. Mol Cell Biol. 1992; 12:3050–9.
47. Kim C, Paulus BF, Wold MS. Interactions of human replication protein A with oligonucleotides. Biochemistry. 1994;33:14197–206.
48. Kim C, Wold MS. Recombinant human replication protein A binds to polynucleotides with low cooperativity. Biochemistry. 1995;34:2058–64.
49. Madireddy A, Gerhardt J. Replication Through Repetitive DNA Elements and Their Role in Human Diseases. In: Masai H, Foiani M, (eds). DNA Replication: From Old Principles to New Discoveries. Singapore: Springer Singapore; 2017. p. 549–81.
50. Sokka M, Rilla K, Miinalainen I, Pospiech H, Syvaoja JE. High levels of TopBP1 induce ATR-dependent shut-down of rRNA transcription and nucleolar segregation. Nucleic Acids Res. 2015;43:4975–89.
51. Delacroix S, Wagner JM, Kobayashi M, Yamamoto K, Karnitz LM. The Rad9-Hus1-Rad1 (9-1-1) clamp activates checkpoint signaling via TopBP1. Genes Dev. 2007;21:1472–7.
52. Lee J, Kumagai A, Dunphy WG. The Rad9-Hus1-Rad1 checkpoint clamp regulates interaction of TopBP1 with ATR. J Biol Chem. 2007;282:28036–44.
53. Lee J, Dunphy WG. Rad17 plays a central role in establishment of the interaction between TopBP1 and the Rad9-Hus1-Rad1 complex at stalled replication forks. Mol Biol Cell. 2010;21:926–35.
54. Mailand N, Gibbs-Seymour I, Bekker-Jensen S. Regulation of PCNA-protein interactions for genome stability. Nat Rev Mol Cell Biol. 2013;14:269–82.
55. Essers J, Theil AF, Baldeyron C, van Cappellen WA, Houtsmuller AB, Kanaar R, et al. Nuclear dynamics of PCNA in DNA replication and repair. Mol Cell Biol. 2005;25:9350–9.
56. Mourelatos D. Sister chromatid exchange assay as a predictor of tumor chemoresponse. Mutat Res Genet Toxicol Environ Mutagen. 2016;803-4:1–12.
57. Luzhna L, Kathiria P, Kovalchuk O. Micronuclei in genotoxicity assessment: from genetics to epigenetics and beyond. Front Genet. 2013;4:131.
58. Yamane K, Tsuruo T. Conserved BRCT regions of TopBP1 and of the tumor suppressor BRCA1 bind strand breaks and termini of DNA. Oncogene. 1999;18:5194–203.
59. Barlow JH, Faryabi RB, Callén E, Wong N, Malhowski A, Chen HT, et al. Identification of early replicating fragile sites that contribute to genome instability. Cell. 2013;152:620–32.
60. Kumar R, Nagpal G, Kumar V, Usmani SS, Agrawal P, Raghava GPS. HumCFS: a database of fragile sites in human chromosomes. BMC Genom. 2019;19:985.
61. Lopez-Flores I, Garrido-Ramos MA. The repetitive DNA content of eukaryotic genomes. Genome Dyn. 2012;7:1–28.
62. Mirkin SM. Expandable DNA repeats and human disease. Nature. 2007;447:932–40.
63. Shastri N, Tsai YC, Hile S, Jordan D, Powell B, Chen J, et al. Genome-wide identification of structure-forming repeats as principal sites of fork collapse upon ATR inhibition. Mol Cell. 2018;72:222–38 e11.
64. Lecona E, Fernandez-Capetillo O. Replication stress and cancer: it takes two to tango. Exp Cell Res. 2014;329:26–34.
65. Lawrence MS, Stojanov P, Mermel CH, Robinson JT, Garraway LA, Golub TR, et al. Discovery and saturation analysis of cancer genes across 21 tumour types. Nature. 2014;505:495.
66. Murga M, Campaner S, Lopez-Contreras AJ, Toledo LI, Soria R, Montana MF, et al. Exploiting oncogene-induced replicative stress for the selective killing of Myc-driven tumors. Nat Struct Mol Biol. 2011;18:1331–5.
67. Schoppy DW, Ragland RL, Gilad O, Shastri N, Peters AA, Murga M, et al. Oncogenic stress sensitizes murine cancers to hypomorphic suppression of ATR. J Clin Investig. 2012;122:241–52.
68. Collins I, Garrett MD. Targeting the cell division cycle in cancer: CDK and cell cycle checkpoint kinase inhibitors. Curr Opin Pharm. 2005;5:366–73.
69. Kaelin WG Jr. The concept of synthetic lethality in the context of anticancer therapy. Nat Rev Cancer. 2005;5:689–98.
70. Tang Z, Li C, Kang B, Gao G, Li C, Zhang Z. GEPIA: a web server for cancer and normal gene expression profiling and interactive analyses. Nucleic Acids Res. 2017;45:W98–W102.
71. Cerami E, Gao J, Dogrusoz U, Gross BE, Sumer SO, Aksoy BA, et al. The cBio cancer genomics portal: an open platform for exploring multidimensional cancer genomics data. Cancer Discov. 2012;2:401.
72. Gao J, Aksoy BA, Dogrusoz U, Dresdner G, Gross B, Sumer SO, et al. Integrative analysis of complex cancer genomics and clinical profiles using the cBioPortal. Sci Signal. 2013;6:pl1.